IEEE Access
Multidisciplinary | Rapid Review | Open Access Journal

Received 19 July 2022, accepted 11 August 2022, date of publication 18 August 2022, date of current version 29 August 2022.

Digital Object Identifier 10.1109/ACCESS.2022.3199696

RESEARCH ARTICLE

Filter Optimization for MFTN-OQAM Systems

NGHIA H. NGUYEN, HA H. NGUYEN, (Senior Member, IEEE), AND BRIAN BERSCHEID
Department of Electrical and Computer Engineering, University of Saskatchewan, Saskatoon, SK S7N 5A9, Canada
Corresponding author: Nghia H. Nguyen (nghia.nguyen@usask.ca)

ABSTRACT In this paper, a novel and effective method for designing the pulse shaping filter for multicarrier faster-than-Nyquist with offset quadrature amplitude modulation (MFTN-OQAM) systems is proposed. The connection between the signal-to-interference ratio (SIR) and the filter coefficients is first established. Then, for a desired overall compression level taking into account compressions in both frequency and time domains, a simple convergence search is suggested to jointly find the optimal values of time and frequency compression factors as well as the filter coefficients to maximize the SIR under a spectrum localization constraint. The obtained results show that higher SIRs, and consequently better bit error rates, can be achieved by the proposed filters over the Martin filter that is commonly used in the filter-bank multicarrier OQAM (FBMC-OQAM) systems (i.e., without time or frequency compression). Moreover, when applying our method to FBMC-OQAM systems, the obtained results show that the original Martin filter is suboptimal as shorter filters are found having the same SIR, which translates to lower implementation cost and latency.

INDEX TERMS Faster-than-Nyquist signaling, FBMC, multicarrier faster-than-Nyquist (MFTN), OFDM, offset QAM (OQAM).

I. INTRODUCTION

The filter-bank multicarrier (FBMC) technique has been studied for many years [1], [2], [3], [4] and is considered as a strong candidate for the physical layer in future wireless communication networks [5], [6]. Compared to the popular orthogonal frequency-division multiplexing (OFDM) technique, a key advantage of FBMC is that it has a much more preferable power spectral density [7], thanks to a well-designed transmit filter [8]. However, FBMC does not provide much data rate enhancement over OFDM. This together with the added complexity are perhaps the reasons that, despite having an excellent spectral property, FBMC has not been widely used in practice.

The multicarrier faster-than-Nyquist (MFTN) technique, first introduced in [9], is a non-orthogonal modulation technique in which one can place data symbols in the time-frequency grid in a flexible manner. Compared to FBMC, MFTN has equally excellent spectrum, but with the added flexibility in controlling the spectral efficiency. This makes MFTN a strong contender against OFDM, FBMC and other orthogonality-based multicarrier transmission techniques.

However, the increase in spectral efficiency comes with a price. By reducing the time interval between consecutive data symbols, severe inter-symbol interference (ISI) occurs, which jeopardizes signal reconstruction at the receiver. Similarly, in the frequency domain, by packing adjacent subcarriers closer together, severe inter-channel interference (ICI) is present. Due to these two sources of interference, MFTN could easily suffer from severe performance degradation even when an ideal channel is considered. As such, a well-designed interference cancellation mechanism is needed for MFTN to obtain acceptable error performance. For example, in [9] and [10], the authors have investigated an MFTN system equipped with an iterative receiver that exploits channel coding for interference cancellation. The theoretical analysis suggests that, with a careful choice of system parameters, MFTN can potentially double the throughput over OFDM. A lower-complexity iterative receiver design is examined in [11] for certain parameters concerning packing data symbols on the time-frequency grid.

It is pointed out that, regardless of the specific interference cancellation technique employed at the receiver, it is always beneficial to design the MFTN system, specifically

The associate editor coordinating the review of this manuscript and approving it for publication was Jie Tang.

the transmit filter, in such a way that there is the least amount of interference in the decision variables (corresponding to the transmitted symbols) at the receiver. In other words, it is sensible to design the transmit filter in the MFTN system to minimize the interference in the decision variables before applying any interference cancellation algorithm. This is precisely the main objective of our work.

There are a few works that consider filter design for single-carrier FTN systems, where the main objective is either optimizing the spectrum shape of the FTN signal [12] or maximizing the signal-to-interference ratio (SIR) [13] at the output of the matched filter. Since MFTN systems enable both faster-than-Nyquist signalling and reduced subcarrier spacing, existing filter designs for single-carrier FTN systems do not necessary perform well when applied to MFTN systems.

As for FBMC, various filter designs have been examined and compared in [14]. The squared-root raised cosine (SRRC) filter and the filter based on the extended Gaussian function (EGF) are examples of filters that perfectly satisfy the Nyquist zero-ISI criterion, provided that the filters are of infinite length. With truncation, their finite impulse response (FIR) versions no longer satisfy the Nyquist zero-ISI criterion [15]. In [16], a flexible design of an FIR filter that aims to satisfy the Nyquist criterion as close as possible is provided. The resulting filter, referred to as squared-root Nyquist (m) filter, is shown to outperform the truncated SRRC filter under timing error (manifested by having a cleaner and wider eye diagram). Perhaps the most widely-used filter is developed in [8], and later refined in [17]. It is generally known as a Martin filter and adopted in the PHYDYAS project [18]. More recently, Martin's design was revisited in [19], and further improved to provide a better out-of-band power suppression ability, and consequently a higher SIR. Nevertheless, all the aforementioned filters are not necessarily good choices for MFTN systems. The main reason is that these filters are designed taking into account the Nyquist zero-ISI criterion, which is no longer relevant in MFTN signalling since MFTN deliberately violates the Nyquist zero-ISI criterion to increase the transmission rate. Furthermore, the impact of compression in the frequency domain is also crucial in MFTN and needs to be accounted for.

Motivated by the above discussion, we propose in this paper a simple, yet effective method to optimize the pulse shaping filter for MFTN systems. Adopting offset quadrature amplitude modulation (OQAM) scheme and Martin's filter structure, we form a direct relationship between the SIR at the output of receive filter and the filter coefficients. By obtaining the gradient of the objective function with respect to the filter coefficients, we are able to perform convergence search to find better filters for various settings of system parameters. In particular, our methods finds new filters that not only yield higher SIRs but also have lower implementation cost and latency for MFTN-OQAM systems when compared to the commonly-used Martin filter. As for FBMC-OQAM, which is a special variant of MFTN-OQAM, our optimization procedure obtains a shorter filter whose SIR performance is the same as that of the original Martin filter.

The remainder of the paper is organized as follows. The system model and SIR derivation for MFTN-OQAM are given in Section II. The formulation of the filter design problem is presented in Section III together with the proposed optimization procedure. Section IV presents and discusses the obtained results. Finally, conclusions are given in Section V.

II. SYSTEM MODEL

The baseband-equivalent transmitted signal of the MFTN-OQAM system under consideration is expressed as follows:

$$x(t) = \sum_{k=0}^{K-1}\sum_{n=0}^{N-1} s_{k,n} \underbrace{e^{j\frac{\pi}{2}(k+n)} g\left(t - n\beta\frac{T}{2}\right) e^{\frac{j2\pi k\alpha t}{T}}}_{\gamma_{k,n}(t)} = \sum_{k=0}^{K-1}\sum_{n=0}^{N-1} s_{k,n}\gamma_{k,n}(t). \quad (1)$$

As in conventional OQAM systems, each complex-valued symbol of duration T is broken up into a pair of real-valued symbols, each of duration $\frac{T}{2}$. In the above expression, K is the number of subcarriers, N is the number of real-valued symbols in one block (frame) and $g(t)$ is the transmit pulse shaping filter. The real-valued symbol carried on the kth subcarrier and over the nth time slot is $s_{k,n}$, whose average energy is normalized to unity, i.e., $E\{s_{k,n}^2\} = 1$. The parameters α and β are the frequency and time compression factors, which control the subcarrier spacing and symbol spacing, respectively.

By sampling with the critical sampling interval $T_{\text{sam}} = \frac{T}{K}$, the discrete-time version of (1) is

$$x[i] \triangleq x(iT_{\text{sam}}) = \sum_{k=0}^{K-1}\sum_{n=0}^{N-1} s_{k,n}\gamma_{k,n}[i], \quad (2)$$

where $\gamma_{k,n}[i] = e^{j\frac{\pi}{2}(k+n)} g\left[i - n\beta\frac{K}{2}\right] e^{\frac{j2\pi k\alpha i}{K}}$. The expression in (2) suggests a block diagram for discrete-time implementation of the transmitter as shown in Fig. 1, in which real-valued symbols enter the transmitter at intervals of $\frac{\beta T}{2}$. The input symbols are upsampled by a factor of $\frac{\beta K}{2}$ to reach the previously mentioned critical sampling interval $T_{\text{sam}} = \frac{T}{K}$ prior to filtering and modulation. Note that while we treat β as a continuous variable in the design of the system, for practical implementation, it should be selected or rounded such that $\beta\frac{K}{2}$ is an integer for implementation.

A popular design of the transmit filter $g[i]$ is based on a weighted sum of Q sinusoids, expressed as

$$g[i] = C\left(a_0 + 2\sum_{q=1}^{Q-1} a_q \cos\left(\frac{2\pi qi}{KL}\right)\right), \quad i = 0, \ldots, KL-1, \quad (3)$$

where L is called the overlapping factor (or filter span in units of symbols) and the length of the filter is KL. In essence, (3)

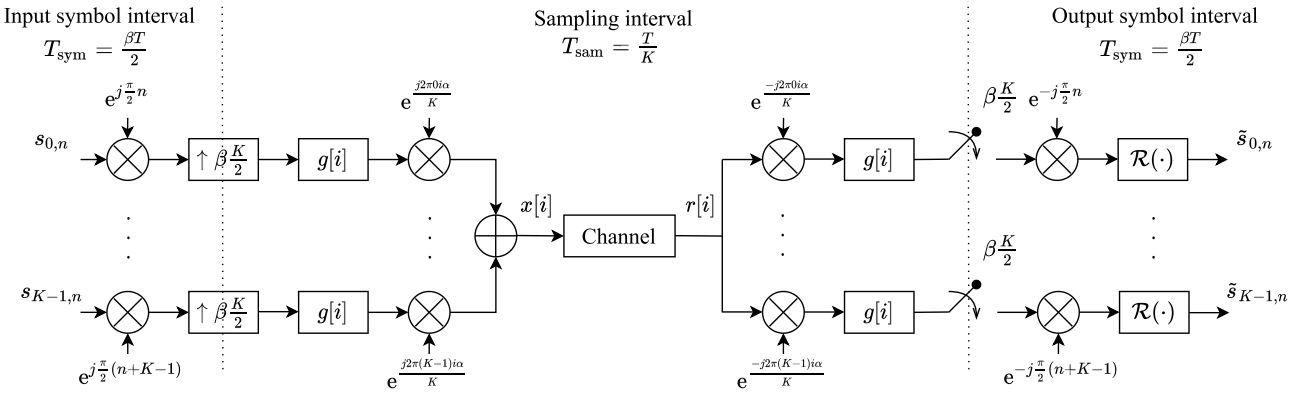

FIGURE 1. Block diagram of the MFTN-OQAM system.

defines the transmit filter through Q *frequency coefficients* a_q. The scaling factor C is chosen to make an unit-energy filter, i.e., $\sum_{i=0}^{KL-1} g^2[i] = 1$. It is noted that the filter defined as in (3) is quite comprehensive in the sense that any filter of length KL can be represented as a combination of $\{a_q\}$. As an example, the simplest filter in the FBMC-OQAM system is designed with $Q = 2$ and $\{a_0, a_1\} = \{1, -1/\sqrt{2}\}$ in [8].

Since the interference caused by the non-orthogonality among the subcarriers and signalling at a faster-than-Nyquist rate is the main performance limiting factor for the MFTN-OQAM system, we are interested in analyzing the interference power. To this end, we focus on the ideal scenario of having a noiseless channel, which means that the received signal is equal to the transmitted signal, i.e., $r[i] = x[i]$. The block diagram for the front-end of the receiver is also shown in Fig. 1. The output of the matched filter corresponding to the mth carrier and lth symbol is

$$\tilde{s}_{m,l} = \mathcal{R}\left\{\sum_{i=0}^{\infty} r[i]\gamma_{m,l}^*[i]\right\} = \mathcal{R}\left\{\sum_{i=l\beta K/2}^{l\beta K/2+KL-1} x[i]\gamma_{m,l}^*[i]\right\}$$
$$= \underbrace{s_{m,l}\Gamma_{(m,l)}^{(m,l)}}_{\text{desired symbol}} + \underbrace{\sum_{(k,n)\neq(m,l)} s_{k,n}\Gamma_{(k,n)}^{(m,l)}}_{\text{interference}}, \tag{4}$$

where

$$\Gamma_{(k,n)}^{(m,l)} = \mathcal{R}\left\{\sum_{i=l\beta K/2}^{l\beta K/2+KL-1} e^{j\frac{\pi}{2}(k+n-m-l)} e^{\frac{j2\pi(k-m)\alpha i}{K}} \times g\left[i - n\beta\frac{K}{2}\right] g\left[i - l\beta\frac{K}{2}\right]\right\} \tag{5}$$

is the cross correlation coefficient between a symbol carried on the kth subcarrier during the nth time slot and another symbol carried on the mth subcarrier during the lth time slot. For convenience, these two symbols shall be referred to as the (k, n)th and (m, l)th symbols, respectively.

Regardless of the detection algorithm, the receiver's performance strongly depends on the signal-to-interference ratio (SIR) at the output of the matched filter. Our main objective is to design the transmit filter (and also the receive filter) to maximize the average SIR. Of course, the design should meet specified constraints on the length and spectrum compactness of the filter. The formulations of the average SIR as a function of the filter coefficients and the filter design problem are presented in the next section.

III. PROBLEM FORMULATION AND OPTIMIZATION PROCEDURE

In order to obtain an expression of the average SIR in terms of the filter coefficients, we focus on the cross correlation coefficient, which can be rewritten as

$$\Gamma_{(k,n)}^{(m,l)} = \mathcal{R}\left\{\sum_{i=0}^{KL-1} e^{j\frac{\pi}{2}(k+n-m-l)} e^{\frac{j2\pi(k-m)\alpha\left(i+\frac{l\beta K}{2}\right)}{K}} \times g\left[i + (l-n)\beta\frac{K}{2}\right] g[i]\right\}. \tag{6}$$

Define a vector of the filter's frequency coefficients $\mathbf{a} = [a_0, \ldots, a_{Q-1}]^\top$. Then, it is simple to show that $[g[0], \ldots, g[KL-1]]^\top = \mathbf{D}_0\mathbf{a}$, in which $\mathbf{D}_0$ is a $KL \times Q$ matrix whose elements are

$$\mathbf{D}_0(u, v) = \cos\left(\frac{2\pi uv}{KL}\right)(2 - 0^v), \tag{7}$$

where $0 \le u \le KL-1$ and $0 \le v \le Q-1$. Next, define a $KL \times Q$ matrix $\mathbf{D}_{(k,n)}^{(m,l)}$ whose element at the uth row and vth column is given in (8), as shown at the bottom of the next page. Then it can be seen that the ith entry of $\mathbf{D}_{(k,n)}^{(m,l)}\mathbf{a}$ is $e^{j\frac{\pi}{2}(k+n-m-l)} e^{\frac{j2\pi(k-m)\alpha\left(i+\frac{l\beta K}{2}\right)}{K}} g\left[i + (l-n)\beta\frac{K}{2}\right]$. Now, (6) can be expressed as

$$\Gamma_{(k,n)}^{(m,l)} = \mathbf{a}^\top \mathbf{D}_{(k,n)}^{(m,l),\top} \mathbf{D}_0\mathbf{a} = \mathbf{a}^\top \mathbf{G}_{(k,n)}^{(m,l)}\mathbf{a}, \tag{9}$$

where $\mathbf{G}_{(k,n)}^{(m,l)} = \mathbf{D}_{(k,n)}^{(m,l),\top}\mathbf{D}_0$.

According to (4), the average power of the desired signal component is

$$P_s(\mathbf{a}) = E\left\{\left(s_{m,l}\Gamma_{(m,l)}^{(m,l)}\right)^2\right\} = E\{s_{m,l}^2\}\left(\Gamma_{(m,l)}^{(m,l)}\right)^2$$

$$= \left(\Gamma_{(m,l)}^{(m,l)}\right)^2 = \left(\mathbf{a}^\top \mathbf{G}_{(m,l)}^{(m,l)} \mathbf{a}\right)^2 = \left(\mathbf{a}^\top \mathbf{G}_0 \mathbf{a}\right)^2, \quad (10)$$

where $\mathbf{G}_0 = \mathbf{G}_{(m,l)}^{(m,l)}$ is a diagonal matrix that is independent of m and l. Specifically, the uth element on the diagonal of $\mathbf{G}_0$ is

$$\mathbf{G}_0(u,u) = \sum_{i=0}^{KL-1} \cos\left(\frac{2\pi iu}{KL}\right)(2-0^i)\cos\left(\frac{2\pi iu}{KL}\right)(2-0^u). \quad (11)$$

This means that the signal power is the same for every symbol in an MFTN-OQAM frame.

On the other hand, for the interference term in (4), denoted as $I_{m,l} = \sum_{(k,n)\neq(m,l)} s_{k,n}\Gamma_{(k,n)}^{(m,l)}$, it is made up of various components caused by symbols transmitted in neighboring subcarriers and adjacent time slots. Statistically, $I_{m,l}$ is a sum of uniformly-distributed random variables with different variances. Given the large number of components in $I_{m,l}$, it can be approximated as a zero-mean Gaussian random variable with variance

$$\sigma_{m,l}^2 = \sum_{(k,n)\neq(m,l)} \left(\Gamma_{(k,n)}^{(m,l)}\right)^2 = \sum_{(k,n)\neq(m,l)} \left(\mathbf{a}^\top \mathbf{G}_{(k,n)}^{(m,l)} \mathbf{a}\right)^2. \quad (12)$$

We define the average SIR as

$$\bar{\xi}(\mathbf{a}) = \frac{P_s(\mathbf{a})}{\frac{1}{KN}\sum_{m=0}^{K-1}\sum_{l=0}^{N-1}\sigma_{m,l}^2} = \frac{KNP_s(\mathbf{a})}{\sum_{m=0}^{K-1}\sum_{l=0}^{N-1}\sum_{(k,n)\neq(m,l)}\left(\mathbf{a}^\top \mathbf{G}_{(k,n)}^{(m,l)}\mathbf{a}\right)^2}. \quad (13)$$

Unlike FBMC-OQAM, the value of $\sigma_{m,l}^2$ varies with l, since $\sigma_{m,l}^2 \neq \sigma_{m,l'}^2$ in general. However, a close examination of (8), (9) and (12) reveals that $\sigma_{m,l}^2 = \sigma_{m,l+\bar{N}}^2$, where $\bar{N}$ is the smallest integer making $\mathcal{R}\left\{\mathbf{D}_{(k,n+\bar{N})}^{(m,l+\bar{N})}\right\} = \mathcal{R}\left\{\mathbf{D}_{(k,n)}^{(m,l)}\right\}$, which is equivalent to making $\frac{\bar{N}\alpha\beta}{2}$ an integer. For example, if $\frac{1}{\alpha\beta} = 1.1$ one finds $\bar{N} = 11$. Using $\bar{N}$, one can simplify the SIR expression to

$$\bar{\xi}(\mathbf{a}) = \frac{K\bar{N}\left(\mathbf{a}^\top \mathbf{G}_0 \mathbf{a}\right)^2}{\sum_{m=0}^{K-1}\sum_{l=\lceil 2L/\beta\rceil}^{\lceil 2L/\beta\rceil+\bar{N}-1}\sum_{(k,n)\neq(m,l)}\left(\mathbf{a}^\top \mathbf{G}_{(k,n)}^{(m,l)}\mathbf{a}\right)^2}. \quad (14)$$

Finally, the optimization of the filter's frequency coefficients to maximize the average SIR can be stated as follows:

$$\arg\max_{\mathbf{a}} \ \bar{\xi}(\mathbf{a}) \quad (15)$$

$$\text{subject to } \mu \geq \mu^*, \quad (16)$$

where $\mu \leq 1$ is the localization ratio that controls the spectral leakage and μ^* is a specified tolerable level of spectral leakage. This ratio is computed as follows:

1) Construct filter $g[i]$ from $\mathbf{a}$
2) Compute DFT $G[k] = \sum_{i=0}^{KL-1} g[i] e^{\frac{j2\pi(k-1)(i-1)}{KL}}$.
3) Among the total KL samples in frequency domain, the in-band components are the first and last $L/2$ samples of $G[k]$, i.e., $G[0:L/2]$ and $G[KL-L/2+1:KL-1]$. The localization ratio μ is then computed as

$$\mu = \frac{\sum_{k=0}^{KL-1}|G^2[k]| - \sum_{k=L/2+1}^{KL-L/2}|G^2[k]|}{\sum_{n=0}^{KL-1}|G^2[k]|}.$$

It is pointed out that the above optimization problem is invariant to the scaling of $\mathbf{a}$. As such, one can arbitrarily set $a_0 = 1$ to reduce one unknown variable. The solution obtained by solving the optimization problem can then be normalized to yield an unit-energy impulse response of the transmit filter.

Maximizing $\bar{\xi}(\mathbf{a})$ is equivalent to minimizing $f = -\bar{\xi}(\mathbf{a})$, which can be expressed as[1]

$$f = -KN_k E_s \underbrace{\frac{1}{\sum_{m=0}^{K-1}\sum_{l=2L}^{2L+N_k-1}\sigma_{m,l}^2}}_{E_1}. \quad (17)$$

The gradient vector of f is

$$\nabla f = -KN_k\left(E_1 \nabla E_s + E_s \nabla E_1\right). \quad (18)$$

The relevant terms in (18) are derived as follows:

$$\nabla E_s = \nabla\left(\mathbf{a}^\top \mathbf{G}_0 \mathbf{a}\right)^2 = 2\left(\mathbf{a}^\top \mathbf{G}_0 \mathbf{a}\right)\nabla\left(\mathbf{a}^\top \mathbf{G}_0 \mathbf{a}\right) = 2\left(\mathbf{a}^\top \mathbf{G}_0 \mathbf{a}\right)2\mathbf{G}_0\mathbf{a}, \quad (19)$$

and

$$\nabla E_1 = \nabla\frac{1}{\sum_{m=0}^{K-1}\sum_{l=2L}^{2L+N_k-1}\sigma_{m,l}^2} = \frac{-\sum_{m=0}^{K-1}\sum_{l=2L}^{2L+N_k-1}\nabla\sigma_{m,l}^2}{\left(\sum_{m=0}^{K-1}\sum_{l=2L}^{2L+N_k-1}\sigma_{m,l}^2\right)^2}, \quad (20)$$

where

$$\nabla\sigma_{m,l}^2 = \sum_{(k,n)\neq(m,l)}\nabla\left(\mathbf{a}^\top \mathbf{G}_{(k,n)}^{(m,l)}\mathbf{a}\right)^2$$

[1]For notational simplicity, the explicit dependence of f on $\mathbf{a}$ is dropped.

$$\mathbf{D}_{(k,n)}^{(m,l)}(u,v) = \begin{cases} \mathcal{R}\left\{e^{j\frac{\pi}{2}(k+n-m-l)} e^{\frac{j2\pi\alpha\left(u+l-\frac{\beta K}{2}\right)(k-m)}{K}}\right\}\cos\left(\frac{2\pi v\left((l-n)\frac{\beta K}{2}+u\right)}{KL}\right)(2-0^v), & 0 \leq \left((l-n)\frac{\beta K}{2}+u\right) \leq KL-1 \\ 0, & \text{otherwise} \end{cases} \quad (8)$$

$$= \sum_{(k,n)\neq(m,l)} 2\left(\mathbf{a}^{\top}\mathbf{G}_{(k,n)}^{(m,l)}\mathbf{a}\right)\left(\mathbf{G}_{(k,n)}^{(m,l)} + \left(\mathbf{G}_{(k,n)}^{(m,l)}\right)^{\top}\right)\mathbf{a}. \tag{21}$$

The final expression for gradient ∇f is given as in (22), shown at the bottom of the next page. With the expression of ∇f, the pseudocode for solving the filter optimization problem is given below.

maxIter $\leftarrow$ 1000 ▷ *Maximum number of iterations*
$c \leftarrow 0$ ▷ *Iteration count*
tolerance $\leftarrow 10^{-10}$ ▷ *Tolerance for* $|\nabla f(\mathbf{a})|$
$S \leftarrow 0.1$ ▷ *Step size*
$\mathbf{a}_n = \mathbf{a}_0$ ▷ *Initialize coefficients*
while $c \leq$ maxIter and $||\nabla f(\mathbf{a}_n)|| \geq$ tolerance **do**
  $\mathbf{a} = \mathbf{a}_n$
  $\mathbf{a}_n = \mathbf{a} - S\nabla f(\mathbf{a})$ ▷ *Update coefficients*
  $S = \frac{|(\mathbf{a}_n - \mathbf{a})(\nabla f(\mathbf{a}_n) - \nabla f(\mathbf{a}))|}{||\nabla f(\mathbf{a}_n) - \nabla f(\mathbf{a})||^2}$ ▷ *Update step size*
  $c = c + 1$
  if $\mu \leq \mu^*$ **then** ▷ *Check spectrum leakage*
    break
  end if
end while
return a

It is pointed out that, since f is a non-convex function, the starting point $\mathbf{a}_0$ plays a crucial role in finding the optimal solution. A reasonable strategy would be to begin with the coefficient set of the Martin filter, although one may find a randomized set of coefficients that yields better results when η increases since the optimized set could be far away from the Martin filter's set. Due to the nature of gradient descent search, multiple trials with different starting points are required to assure that the global optimal solution is obtained.

IV. RESULTS AND DISCUSSIONS

A. SIR IMPROVEMENTS

In this section, the filters obtained by the proposed optimization are presented for several configurations of the MFTN-OQAM systems. The number of subcarriers is set to $K = 32$, whereas the overlapping factor is either $L = 3$ or $L = 4$, which are the two most widely-used values in FBMC-OQAM. The spectral efficiency is determined as $\eta = \frac{R\log_2(M)}{\alpha\beta}$ (bits/s/Hz), where M and R are the modulation order and the coding rate, respectively. As one can see, for fixed code rate R and modulation order M, different gains in spectral efficiency can be obtained for MFTN by adjusting the product $\alpha\beta$. In contrast, the spectral efficiency of FBMC is fixed at $R\log_2(M)$ (bits/s/Hz). Furthermore, since M and R do not affect the calculation of the average SIR, one can set $R = 0.5$ and $M = 4$, which means $s_{k,n} \in \{-1, 1\}$. For all the results presented in this section, the tolerable level of spectral leakage is specified as $\mu^* = 95\%$.

First, the optimization algorithm is performed for the case that the number of filter's frequency coefficients is equal to the overlapping factor, i.e., $Q = L$. Although not necessarily an ideal choice, it has been widely adopted in the literature of FBMC-OQAM [8]. In particular, for the case $Q = L = 3$, the frequency coefficients of the Martin filter obtained in [8] for FBMC-OQAM is $\mathbf{a}_0 = [1, -0.91143783, 0.41143783]$.

Practically, spectral efficiency (which is controlled through the product $\alpha\beta$) is often specified as one of the design targets, and then one should choose α and β accordingly to maximize the SIR for the specified spectral efficiency. Therefore, with each value of η, the optimization algorithm refines $\mathbf{a}_n$ and outputs the optimized $\mathbf{a}$ as shown in Table 1. The table also compares the SIR values between the optimized filter and the original Martin filter for the same set of compression factors (α, β). It can be seen that for all combinations of (α, β), our optimized filters always perform better than the Martin filter, especially when η is close to 1. For example, a gain of 1.5 dB is achieved when using the proposed filter for $\eta = 1$ (i.e., a FBMC-OQAM system). On the other hand, a gain of 2.1 dB is obtained by the proposed filter for $\eta = 1.1$.

Similar SIR improvements are obtained with the filters optimized with $Q = L = 4$ and reported in Table 2, in which the largest SIR gain is observed when $\eta = 1.1$. The coefficients of the original Martin filter designed for FBMC-OQAM systems are $\mathbf{a}_0 = [1, -0.97195983, \sqrt{2}/2, -0.23514695]$ [8]. Since the filter length is larger in this case (with $L = 4$), the average SIRs are higher than those in Table 1 (with $L = 3$). It is worth pointing out that, even for an FBMC-OQAM system, the proposed filter always provides SIR improvement over the original Martin filter, regardless of filter length.

As discussed before, the number of filter's frequency coefficients Q needs not be the same as the overlapping factor L, nor does it affect the length (hence complexity) of the filter in the time domain. In fact, one should use a large value for Q in order to have more flexibility in optimizing the spectrum of the filter, and consequently achieve higher SIR. This is easily explored with the proposed optimization algorithm and the results are presented in Fig. 2 for $\eta = 1$ (corresponding to an FBMC system) and two different values of L. It can be seen that, for the case $L = 3$, using $Q = L = 3$ delivers the maximum SIR of 43 dB, whereas the maximum SIR increases to 68 dB with $Q = 7$, i.e., a gain of 25 dB over the conventional Martin filter. The optimized filter's frequency coefficients found with $Q = 7$ are $\mathbf{a} = [1, -0.8868850, 0.5412187, -0.2014944, 0.0415070, 0.0254808, -0.0201625]$. Similarly, for the case of $L = 4$, the maximum SIR jumps from 65 dB to 88 dB when switching from $Q = 4$ to $Q = 8$. The filter's frequency coefficients found with $Q = 8$ are $\mathbf{a} = [1, -0.9518146, 0.7071373, -0.3011248, 0.0074495, 0.0561705, -0.0000126, -0.0177636]$. Although the optimization algorithm can also find optimal filters for the cases $\eta > 1$ (corresponding to MFTN systems), no significant improvements in SIR are observed by increasing the number of filter's frequency coefficients $(Q > L)$ in those cases. As a result, our proposed method can be used to obtain optimized

TABLE 1. Optimal combinations of $\{\alpha, \beta, \mathbf{a}\}$ to maximize $\bar{\xi}$ when $Q = L = 3$.

η	Optimized filter α	β	$\mathbf{a}$	$\bar{\xi}$ (dB)	Original Martin filter α	β	$\bar{\xi}$ (dB)
1	1	1	$[1, -0.9165333, 0.4014513]$	44.9	1	1	43.4
1.1	0.9697	0.9375	$[1, -0.9637144, 0.1458119]$	8.4	0.9697	0.9375	6.3
1.2	0.9524	0.875	$[1, -0.9551031, 0.1830014]$	6.6	0.9524	0.875	5.4
1.3	0.9467	0.8125	$[1, -0.9475810, 0.2244483]$	5.1	0.9467	0.8125	4.6
1.4	0.9524	0.75	$[1, -0.9384733, 0.2763826]$	4	0.9524	0.75	3.8

TABLE 2. Optimal combinations of $\{\alpha, \beta, \mathbf{a}\}$ to maximize $\bar{\xi}$ when $Q = L = 4$.

η	Optimized filter α	β	$\mathbf{a}$	$\bar{\xi}$ (dB)	Original Martin filter α	β	$\bar{\xi}$ (dB)
1	1	1	$[1, -0.9719183, 0.7073757, -0.2362098]$	66.7	1	1	65.2
1.1	0.9697	0.9375	$[1, -1.0951204, 0.6059836, 0.02505963]$	8.8	0.9697	0.9375	6.6
1.2	0.9524	0.875	$[1, -1.0621831, 0.6204143, 0.0004637]$	6.7	0.9524	0.875	5.6
1.3	0.9467	0.8125	$[1, -1.0269941, 0.6367087, -0.0344359]$	5.2	0.9427	0.8125	4.7
1.4	0.9524	0.75	$[1, -0.9977191, 0.6576806, -0.0824836]$	4	0.9524	0.75	3.9

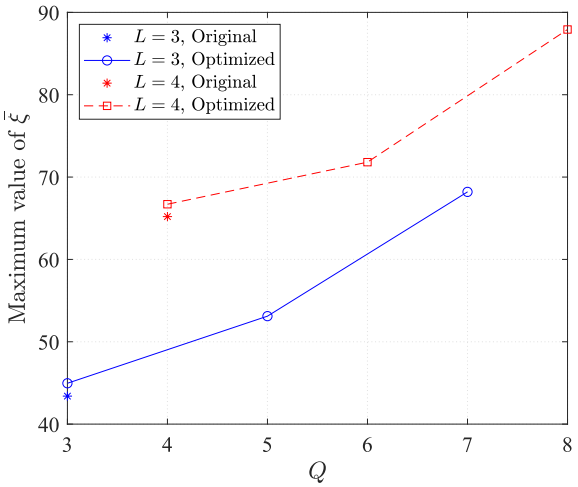

FIGURE 2. Maximum $\bar{\xi}$ versus the number of filter's frequency coefficients.

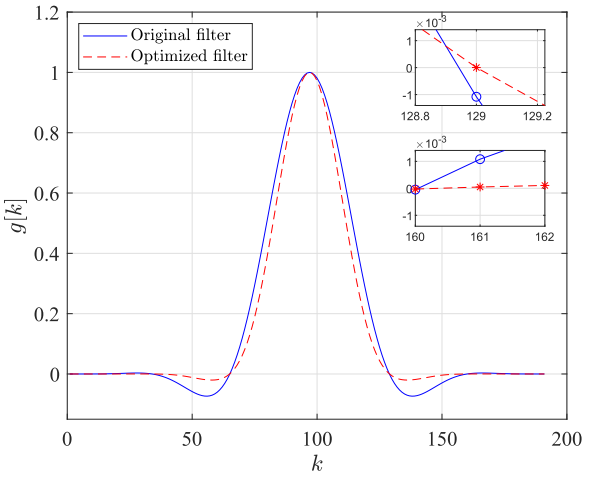

FIGURE 3. Impulse responses of cascaded filters, $L = 3$.

filters for MFTN-OQAM by setting $Q = L$, since using higher values of Q is practically unnecessary.

B. FILTER RESPONSES

In this part, the original Martin filter and the optimized filter are compared in terms of ISI immunity and spectrum localization. Consider an FBMC-OQAM system (i.e., an MFTN-OQAM system with $\alpha = \beta = 1$) with $K = 32$ and $L = 3$. For each design, the impulse response of the cascaded transmit-receive filter is plotted in Fig. 3. Recall that the original Martin filter achieves $\bar{\xi} = 43.4$ dB, whereas the optimized filter has $\bar{\xi} = 68$ dB. As expected, both cascaded filters peak at $KL + 1 = 97$. At samples $KL + 1 + iK$, the optimized filter satisfies the zero-ISI criterion better than the original filter, with amplitude difference of 10^{-3}.

$$\nabla f = KN_k \frac{\left(\mathbf{a}^\top \mathbf{G}_0 \mathbf{a}\right)^2}{\left(\sum_{m=0}^{K-1} \sum_{l=2L}^{2L+N_k-1} \sigma_{m,l}^2\right)^2} \sum_{m=0}^{K-1} \sum_{l=2L}^{2L+N_k-1} \sum_{k,n} 2\left(\mathbf{a}^\top \mathbf{G}_{(k,n)}^{(m,l)} \mathbf{a}\right)\left(\mathbf{G}_{(k,n)}^{(m,l)} + \left(\mathbf{G}_{(k,n)}^{(m,l)}\right)^\top\right)\mathbf{a}$$
$$+KN_k \frac{2\left(\mathbf{a}^\top \mathbf{G}_0 \mathbf{a}\right) 2\mathbf{G}_0 \mathbf{a}}{\sum_{m=0}^{K-1} \sum_{l=2L}^{2L+N_k-1} \sum_{k,n} \left(\mathbf{a}^\top \mathbf{G}_{(k,n)}^{(m,l)} \mathbf{a}\right)^2}. \tag{22}$$

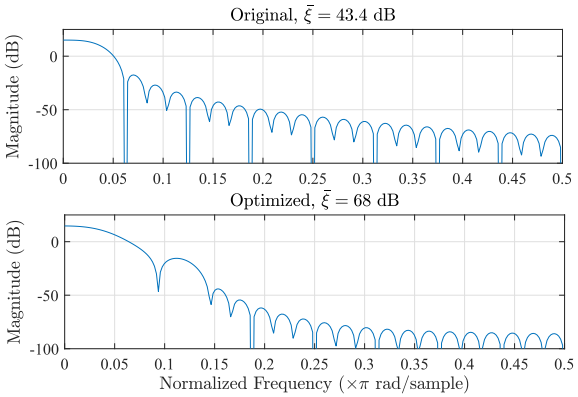

FIGURE 4. Magnitude responses of two transmit filters under comparison, $L = 3$.

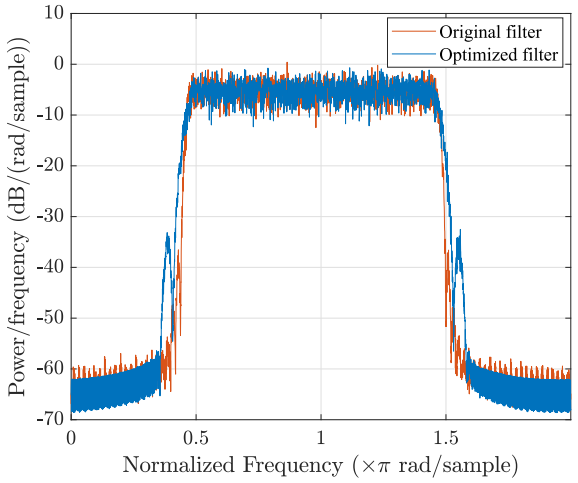

FIGURE 5. PSDs of transmit FBMC-OQAM signals with two different filter designs, $L = 3$.

Compared to the original Martin filter, the optimized filter has poorer spectral localization as shown in Fig. 4. Specifically the stopband of the optimized filter is wider and there is a notable sidelobe next to the passband of the filter. However, it is stressed that the relevant and important assessment is the power spectrum density (PSD) of the FBMC-OQAM signal, which is shown in Fig. 5 for both filter designs. Although having higher spectral sidelobes, the overall PSD obtained with the proposed filter has very sharp transition band and very low amount of out-of-band power emission.

Similar observations can be made from Figs. 6, 7 and 8 for the case $L = 4$. In Fig. 6, the cascaded response of the optimized filter is infinitesimal at samples $KL + 1 + iK$, with the difference of 2×10^{-4}. Figs. 7 and 8 show some deteriorations of the magnitude response and PSD of the optimized filter compared to the original Martin filter. However, such deteriorations can be well justified by the much better ISI immunity, and consequently by the much better overall SIR.

C. BIT ERROR RATES

Next, we investigate how the SIR improvement translates to the bit error rate (BER) performance when the optimized

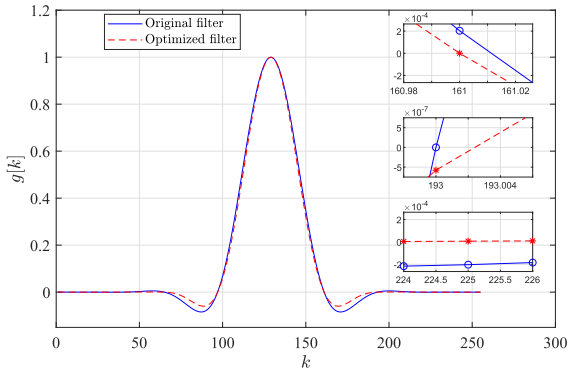

FIGURE 6. Impulse responses of cascaded filters, $L = 4$.

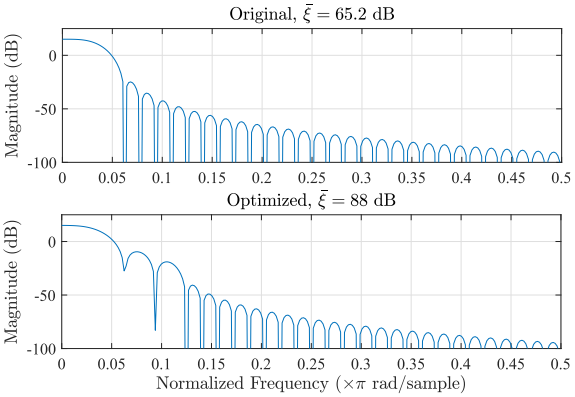

FIGURE 7. Magnitude responses of two transmit filters under comparison, $L = 4$.

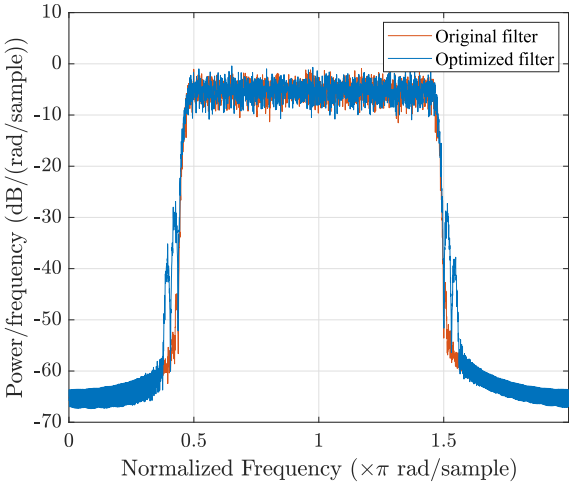

FIGURE 8. PSDs of transmit FBMC-OQAM signals with two different filter designs, $L = 4$.

filters are compared to the original Martin filter. To this end, we obtain the BER over an additive white Gaussian noise (AWGN) channel for systems that implement a rate $R = 1/2$ convolutional code with constraint length 10, whose generator matrix is [2473, 3217] in octal form. The coded sequence is mapped to symbols $s_{k,n}$ using the standard

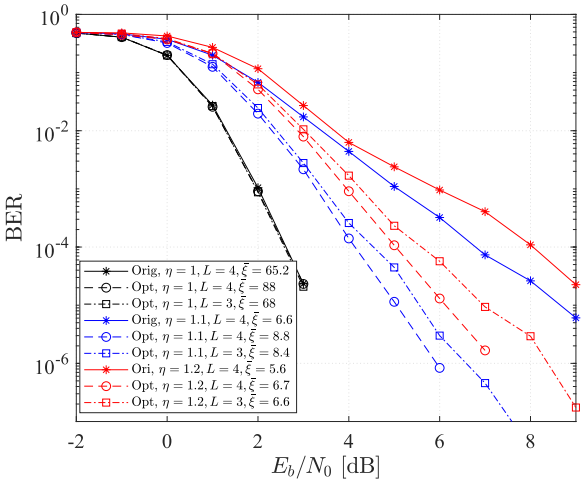

FIGURE 9. BER comparison of different MFTN-OQAM systems.

QPSK constellation and Gray mapping. At the receiver, the soft-input hard-output Viterbi algorithm is implemented to decode the log-likelihood ratio of the demodulated binary sequence. It is noted that no interference cancelation method is implemented before channel decoding. This is to observe the gross performance improvement in terms of BER with the optimized filters.

As can be seen in Fig. 9, when $\eta = 1$ and $L = 4$, the use of both original and optimized filters leads to virtually identical BER performance. This is because the average SIR resulting from using these two filters are very high, making the interference insignificant compared to thermal noise. For the same reason, the BER performance of the system using the optimized filter with $L = 3$ (which achieves an SIR of about 68 dB) is equivalent to the two filters having $L = 4$. This comparison means that our filter optimization algorithm reduces the filter length by 25%, from $4K$ to $3K$, without sacrificing the error performance.

When $\eta = 1.1$, the SIR gain helps to improve the BER. Specifically, it can be seen from Fig. 9 that the optimized filters with both $L = 3$ and $L = 4$ deliver better BER performance compared to the original filter designed with $L = 4$. At the BER level of 10^{-5}, a 4 dB gain is achieved with the optimized filter designed with $L = 4$ over the original filter of the same length. Note that the SIR improvement between these two filters is about 2.2 dB as discussed before. Similar observation can be made when $\eta = 1.2$. The SIR improvement of 1.1 dB translates to 3.2 dB gain in E_b/N_0 at the BER level of 2×10^{-5}. The results clearly show that the optimized filters are preferred over the original filters when the system is designed for a higher spectral efficiency ($\eta > 1$).

V. CONCLUSION

This paper has formulated and solved the filter design problem for multicarrier faster-than-Nyquist (MFTN) systems with offset quadrature amplitude modulation (OQAM). With the objective of maximizing the signal-to-interference ratio (SIR) at the output of the matched filter, the frequency coefficients of the transmit filter are found that meet a criterion on spectral localization and for a fixed spectral efficiency. The obtained results showed that the optimized filters can boost SIR up to 25 dB in the orthogonal multicarrier systems (FBMC-OQAM), and up to 2.2 dB for non-orthogonal MFTN-OQAM systems that implement compression factors to increase the spectral efficiency. The BER results have also confirmed the usefulness of the optimized filters and showed that, for the non-orthogonal MFTN-OQAM systems, the SIR improvement translates to a larger power gain by using the optimized filters. Future works could investigate the MFTN-OQAM systems with the optimized filters under other channel models, as well as with more advanced receivers. The extension of this work to multiple-input multiple-output (MIMO) systems is interesting, considering that filter design can help reduce intrinsic interference that is more problematic with MIMO channels. Such an extension is beyond the scope of this work and deserves a further and extensive study.

REFERENCES

[1] H. S. Malvar, "Extended lapped transforms: Properties, applications, and fast algorithms," *IEEE Trans. Signal Process.*, vol. 40, no. 11, pp. 2703–2714, Nov. 1992.

[2] M. G. Bellanger, "Specification and design of a prototype filter for filter bank based multicarrier transmission," in *Proc. IEEE Int. Conf. Acoust., Speech, Signal Process.*, May 2001, pp. 2417–2420.

[3] P. Siohan, C. Siclet, and N. Lacaille, "Analysis and design of OFDM/OQAM systems based on filterbank theory," *IEEE Trans. Signal Process.*, vol. 50, no. 5, pp. 1170–1183, May 2002.

[4] P. Singh, H. B. Mishra, A. K. Jagannatham, K. Vasudevan, and L. Hanzo, "Uplink sum-rate and power scaling laws for multi-user massive MIMO-FBMC systems," *IEEE Trans. Commun.*, vol. 68, no. 1, pp. 161–176, Jan. 2020.

[5] F. Schaich and T. Wild, "Waveform contenders for 5G—OFDM vs. FBMC vs. UFMC," in *Proc. 6th Int. Symp. Commun., Control Signal Process. (ISCCSP)*, May 2014, pp. 457–460.

[6] A. F. Demir, M. Elkourdi, M. Ibrahim, and H. Arslan, "Waveform design for 5G and beyond," in *5G Networks: Fundamental Requirements, Enabling Technologies, and Operations Management*. Hoboken, NJ, USA: Wiley, Sep. 2018, pp. 51–76.

[7] B. Farhang-Boroujeny, "OFDM versus filter bank multicarrier," *IEEE Signal Process. Mag.*, vol. 28, no. 3, pp. 92–112, May 2011.

[8] K. W. Martin, "Small side-lobe filter design for multitone data-communication applications," *IEEE Trans. Circuits Syst. II, Analog Digit. Signal Process.*, vol. 45, no. 8, pp. 1155–1161, Aug. 1998.

[9] F. Rusek and J. B. Anderson, "Multistream faster than Nyquist signaling," *IEEE Trans. Commun.*, vol. 57, no. 5, pp. 1329–1340, May 2009.

[10] F. Rusek and J. B. Anderson, "Successive interference cancellation in multistream faster-than-Nyquist signaling," in *Proc. Int. Conf. Commun. Mobile Comput. (IWCMC)*, Jul. 2006, pp. 1021–1026.

[11] S. Peng, A. Liu, X. Liu, K. Wang, and X. Liang, "MMSE turbo equalization and detection for multicarrier faster-than-Nyquist signaling," *IEEE Trans. Veh. Technol.*, vol. 67, no. 3, pp. 2267–2275, Mar. 2018.

[12] S. B. Makarov, M. Liu, A. S. Ovsyannikova, S. V. Zavjalov, I. I. Lavrenyuk, W. Xue, and J. Qi, "Optimizing the shape of Faster-than-Nyquist (FTN) signals with the constraint on energy concentration in the occupied frequency bandwidth," *IEEE Access*, vol. 8, pp. 130082–130093, 2020.

[13] Q. Chen and H. Zhang, "Shaping filter design for Faster-than-Nyquist signaling with second order polynomial function," in *Proc. Int. Conf. Cyber-Enabled Distrib. Comput. Knowl. Discovery*, Sep. 2015, pp. 442–445.

[14] A. Sahin, I. Guvenc, and H. Arslan, "A survey on multicarrier communications: Prototype filters, lattice structures, and implementation aspects," *IEEE Commun. Surveys Tuts.*, vol. 16, no. 3, pp. 1312–1338, 3rd Quart., 2014.
[15] P. Siohan and C. Roche, "Cosine-modulated filterbanks based on extended Gaussian functions," *IEEE Trans. Signal Process.*, vol. 48, no. 11, pp. 3052–3061, Nov. 2000.
[16] B. Farhang-Boroujeny, "A square-root Nyquist (M) filter design for digital communication systems," *IEEE Trans. Signal Process.*, vol. 56, no. 5, pp. 2127–2132, May 2008.
[17] S. Mirabbasi and K. Martin, "Overlapped complex-modulated transmultiplexer filters with simplified design and superior stopbands," *IEEE Trans. Circuits Syst. II, Analog Digit. Signal Process.*, vol. 50, no. 8, pp. 456–469, Aug. 2003.
[18] M. Bellanger, "FBMC physical layer: A primer," PHYDYAS Project, Tech. Rep., Jun. 2010. [Online]. Available: http://www.ict-phydyas.org/teamspace/internal-folder/FBMC-Primer_06-2010.pdf
[19] R. T. Kobayashi and T. Abrao, "FBMC prototype filter design via convex optimization," *IEEE Trans. Veh. Technol.*, vol. 68, no. 1, pp. 393–404, Jan. 2019.

NGHIA H. NGUYEN received the B.E. degree in electrical engineering from the Hanoi University of Science and Technology (HUST), Hanoi, Vietnam, in 2018, and the M.S. degree in electrical engineering from the University of Saskatchewan, Saskatoon, Canada, where he is currently pursuing the Ph.D. degree. His research interests include multicarrier systems and faster-than-Nyquist signaling.

HA H. NGUYEN (Senior Member, IEEE) received the bachelor's degree from the Hanoi University of Technology (HUT), Hanoi, Vietnam, in 1995, the master's degree from the Asian Institute of Technology (AIT), Bangkok, Thailand, in 1997, and the Ph.D. degree from the University of Manitoba, Winnipeg, MB, Canada, in 2001, all in electrical engineering.

He joined the Department of Electrical and Computer Engineering, University of Saskatchewan, Saskatoon, SK, Canada, in 2001, and became a Full Professor, in 2007. He is currently holding the position of the NSERC/Cisco Industrial Research Chair of Low-Power Wireless Access for Sensor Networks. He is the coauthor, with Ed Shwedyk, of the textbook *A First Course in Digital Communications* (Cambridge University Press). His research interests include the broad areas of communication theory, wireless communications, and statistical signal processing.

Dr. Nguyen is a fellow of the Engineering Institute of Canada (EIC) and a Registered Member of the Association of Professional Engineers and Geoscientists of Saskatchewan (APEGS). He served as the technical program chair for numerous IEEE events. He was the General Chair of the 30th Biennial Symposium on Communications, in 2021. He was an Associate Editor of the IEEE TRANSACTIONS ON WIRELESS COMMUNICATIONS and IEEE WIRELESS COMMUNICATIONS LETTERS, from 2007 to 2011 and, from 2011 to 2016, respectively. He is currently serving as an Associate Editor for the IEEE TRANSACTIONS ON VEHICULAR TECHNOLOGY and IEEE TRANSACTIONS ON COMMUNICATIONS.

BRIAN BERSCHEID received the B.E. and Ph.D. degrees in electrical engineering from the University of Saskatchewan, Saskatoon, SK, Canada, in 2006 and 2011, respectively.

From 2006 to 2017, he was with Vecima Networks, where he designed broadband cable access equipment and researched next-generation access technologies. In 2017, he joined the Department of Electrical and Computer Engineering, University of Saskatchewan, as the Barbhold Chair of Information Technology and an Assistant Professor. He is currently licensed as a Professional Engineer with the Association of Professional Engineers and Geoscientists of Saskatchewan. His research interests include the design and implementation of algorithms for communications, signal processing, and machine learning.